APPROACHES TO ELECTROMAGNETIC SIMULATIONS OF ADVANCED SERS SUBSTRATES

Pavel KWIECIEN, Jan FIALA, Lucie ŠTOLCOVÁ, Jan PROŠKA, Ivan RICHTER

Czech Technical University in Prague, Faculty of Nuclear Sciences and Physical Engineering,
Department of Physical Electronics, Břehová 7, 11519 Prague 1, Czech Republic

Abstract

Today, the techniques based on the phenomenon of surface-enhanced Raman scattering (SERS) has been finding many interesting applications. Although not fully understood yet, prevailing explanation takes account of electromagnetic and chemical contributions to Raman scattering "amplification", with the enhancement factor spanning several orders of magnitude, when molecules under investigation are adsorbed on metal nanoparticles or more complex nanostructured metal surfaces (called SERS-active substrates). Two main requirements for high-quality SERS substrates include large enhancement factors (mainly in small regions called hot spots) and homogeneity of substrates. Concerning possible morphology and design of SERS structures, there are several design strategies available, with the experimental technique, based on self-assembly approaches, belonging to the most progressive ones. Also, apart from low cost and possibility to create large surfaces, this technique additionally provides another important issue, the morphology-based tunability of optical properties of these substrates. Recently, in our department, the experimental techniques and preparation procedures based on the bottom-up approach using self-assembly technique have been mastered and successfully applied to periodic SERS substrate preparation. In this way, series of various reproducible periodic arrays of semishells, nanobowls, and other types of substrates have been prepared, characterized, and tested under SERS measurements in recent years. These structures are indeed one of good candidates for "best" SERS-active substrates. Concerning the complexity and rich physics of such structures, advanced numerical electromagnetic techniques are required for reliable numerical studies and predictions of structural behavior. Such detailed simulations, helping to understand the undergoing physics, have not mostly been available yet. Hence, in this contribution, we present our recent studies on the electromagnetic modeling of two promising types of advanced SERS substrates with the rigorous 3D finite difference time domain (FDTD) technique.

Keywords:

Raman spectroscopy, SERS-active substrate, surface plasmon, electromagnetic field enhancement, FDTD

1. INTRODUCTION

Recently, spectroscopy technique based on surface-enhanced Raman scattering (SERS) has found, as a promising and versatile method, many potential applications [1,2]. Since the cross-sections of standard Raman scattering processes are extremely weak, such enhancement mechanism (by several orders of magnitude) is indeed needful. SERS-active substrates, i.e. substrates with noble metal nanostructures distributed in close proximity of studied compounds, have undergone enormous progress in last couple of years. Thus, although the detailed principles of SERS functioning still remain not completely understood [2], the SERS-based analytical technique, using SERS-active substrates, appears a versatile tool in chemical and biomedical sensing [3], with several crucial advantages, such as low detection limits, fast procedure, possibility of non-destructive *in-situ* analysis with structural information of the analyte, *etc*. For such substrates, advanced plasmonic nanostructures (see, *e.g.* [4-8]) are fruitfully employed. Among them, structures belonging either to the family of plasmonic shells and semishells [8-13] or to triangular structures [14-15] have appeared as the most efficient and perspective ones. However, in contrast to extensive experimental activities in this area, including the successful development and mastering of efficient preparation techniques for both types of structures in our laboratory [16-18], there is still lack of reliable and thorough simulation activities, with only few exceptions (e.g. [19]). Clearly, there is an urge for such theoretical analysis, with respect to both description of the behavior, as well as prediction of new substrate arrangements. This is also the attempt of this paper. Apart from global characteristics (cross sections and reflection / transmission spectral dependences), as a proper characteristic of the amplification of the field in the vicinity of a localized plasmonic nanostructure, we have also opted for the enhancement factor (EF), defined as the properly normalized forth power of the local electromagnetic field [2].

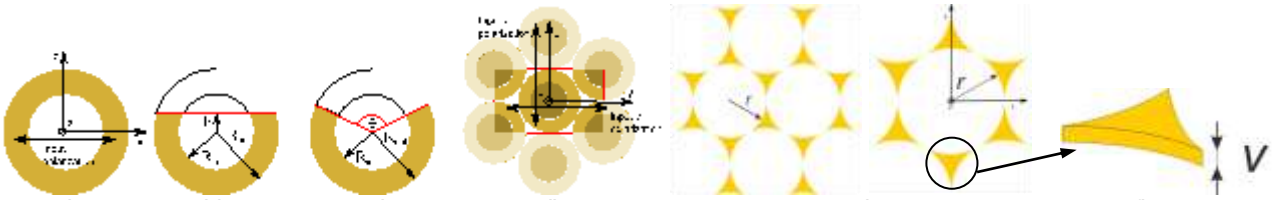

a) b) c) d) e) f)

Fig. 1: Schematic of gold semishell and triangular structures considered in simulations: a) a fully covered nanoshell structure with an air core; b) a semishell with parallel opening; c) a semishell with conical opening; d) example of periodic two-dimensional close-packed array of semishells; e) array of triangular structures; f) detail of an isolated triangle structure. In both cases, the arrangement with hexagonal symmetry is considered, with indication of the simulation cell and coordinate system.

2. SIMULATION RESULTS AND DISCUSSION

In this section, we present the computer numerical modeling results, obtained with the three-dimensional finite difference time domain algorithm (FDTD Solutions, from Lumerical Solutions [20]), of the electromagnetic response of our structures of interest. Two types of structures were studied: (1) gold semishells, in both isolated and periodic arrangements (Fig.1b) - d)), and (2) gold triangular structures (Fig.1e) and f)), in direct resemblance with prepared structures. As the permittivity of gold, the data taken from Johnson and Christy were used [21]. Concerning the semishells, first, isolated structures were numerically examined, in terms of the corresponding extinction cross sections (and thus absorption and scattering cross sections), together with the electromagnetic field profile distributions, presented in the form of the corresponding enhancement factor. Next, the analysis of a periodic two-dimensional close-packed array with hexagonal arrangement (see Fig.1d) was considered. In our simulations, we have applied the following parameters: diameter of Au semishells R_{out} = 100 nm, thickness d of Au walls (i.e. the difference between $d = R_{out} - R_{in}$, see Fig.1b) 20 nm. As a tuning parameter, the height h (measured from the center, see Fig.1b) of a semishell was changed appropriately. Although not presented in the paper, due to space limitations, we have changed the diameter and wall thickness, too. With FDTD calculations, after testing, we have chosen the resolution in the computational domain well below 1 nm resolution, to ensure proper convergence of the results. For isolated structures, total field / scattered field technique was used, in combination with perfectly matched layers (PML), as proper boundary conditions, applied to all sides of a computational window, whereas for periodic structures, periodic boundary conditions were applied for the vertical walls and PML to horizontal ones.

For isolated semishell structures (located in air environment, with no substrate) with parallel opening (see Fig.1b)), the extinction, absorption, and scattering cross section spectral dependences are shown in Fig.3, for several heights h and angles θ as parameters, for the input field polarization chosen along x axis (perpendicular incidence). It should be noted that this choice of polarization is only technical, due to rotational symmetry of the isolated structure. As can be seen in Fig. 3, both types of structures perform similarly well, with distinct extinction peaks. Two distinct plasmon resonances are clearly visible due to a reduced symmetry of a structure, axial mode and transverse mode.

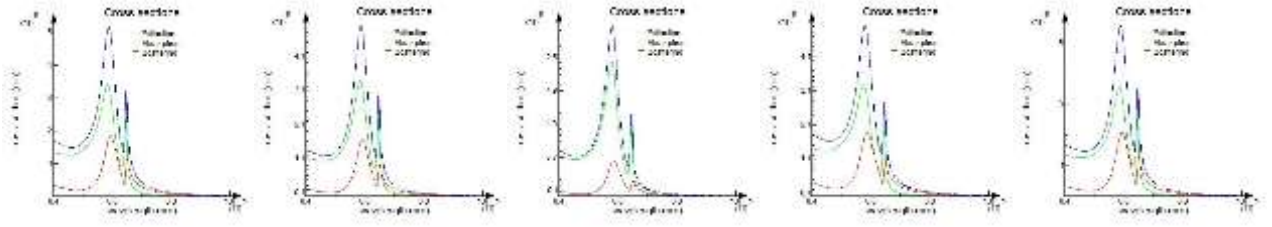

a) b) c) d) e)

Fig. 3: Extinction, absorption, and scattering cross sections of an isolated gold semishell with parallel (Fig. 1b) and conical (Fig.1c) opening: a) h = 20 nm; b) semishell with h = 0 nm (halfshell); c) semishell with h = -20 nm; d) θ = 90 deg; e) θ = 120 deg. Structure diameter R_{out} = 100 nm, d = 20 nm, input field polarization along x axis, h and θ are given in Fig.1b).

Next, we have concentrated on the detailed analysis of the field enhancement factor, imaged in the zx plane; see Fig.4 (note the log scale used). Here, the same h parameters, as in Fig.3, were selected, and the EF was plotted for the wavelengths corresponding to the extinction maxima (Fig.4b), d), f), h) and j)). However, it has turned out that the maxima of the EF do not directly correspond to the extremes of the extinction cross sections. Thus, we have also added the EF plots for such wavelengths where they are maximized (Fig.4a),

c), e), g) and i)). In figures, localized maxima of the EF are clearly seen (red color, located at either inner or both sides of the semishell walls, depending on the particular choice of *h*), corresponding to hot spots of the SERS maximum enhancement, due to the parallel orientation of the input polarization and the zx plane. As can be seen, the maximum EF (as high as 10^5) is achievable for all choices of structure heights with corresponding wavelengths (see Fig.4a),c),e),h). This reflects a rather good flexibility in the design, with respect to practical realization technique.

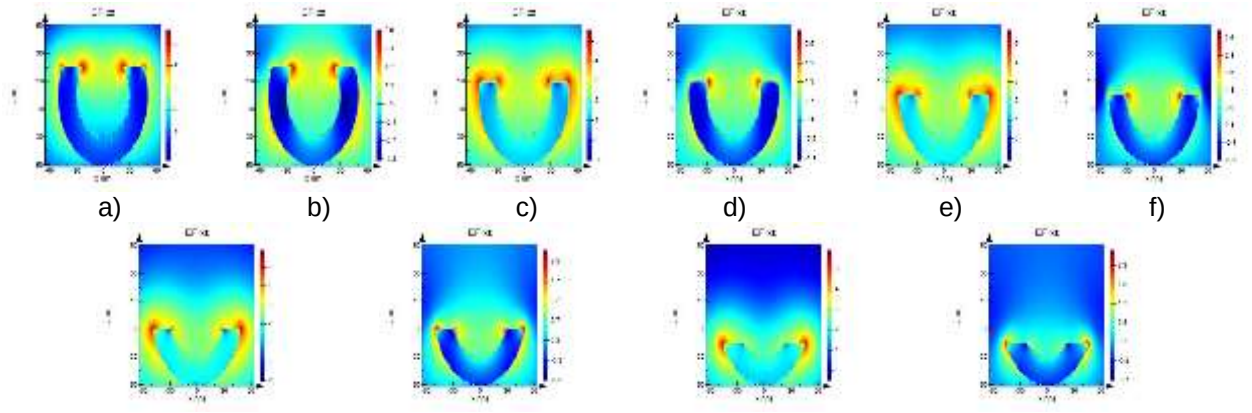

Fig. 4: Field enhancement factors (EF) in zx plane for the gold semishell structure from Fig.1b) (R_{out} = 100 nm, *d* = 20 nm, log scale): a) semishell with *h* = 20 nm (λ = 710 nm – EF maximum); b) *h* = 20 nm (λ = 589 nm – extinction maximum); c) *h* = 10 nm (λ = 726 nm – EF); d) *h* = 10 nm (λ = 589 nm – extinction); e) *h* = 0 nm (λ = 762 nm – EF); f) *h* = 0 nm (λ = 585 nm – extinction); g) *h* = -10 nm (λ = 722 nm – EF); h) *h* = -10 nm (λ = 585 nm – extinction); i) *h* = -20 nm (λ = 718 nm – EF); and j) *h* = -20 nm (λ = 581 nm – extinction); input x polarization.

Such hot spots in the EF are, however, clearly not obtained for the perpendicular cuts in zy plane; see Fig.5, where the corresponding EF distributions are shown, with the same meaning and notation as in Fig.4. As can be seen, in this plane, the EF distribution now does not form the localized hot spots, and is only rather homogeneously enhanced in the inner area of the semishell.

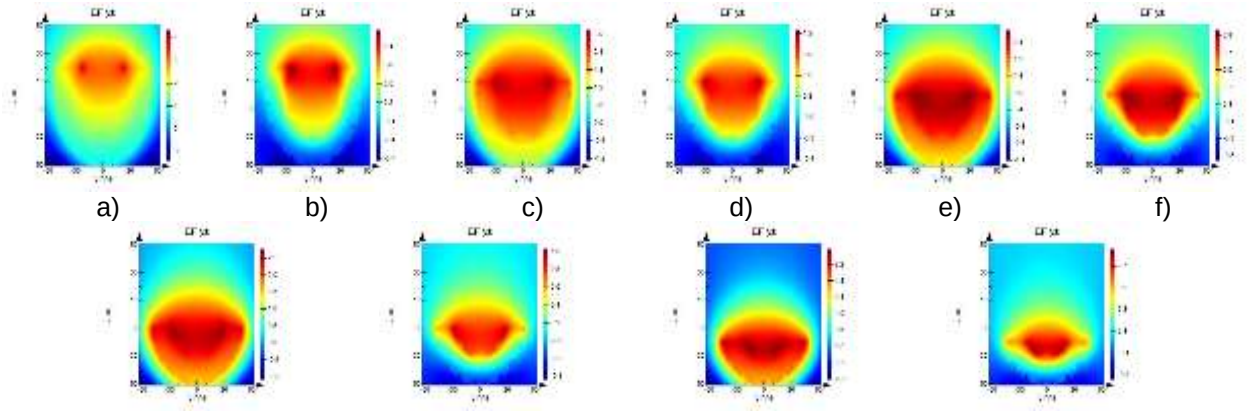

Fig. 5: Field enhancement factors (EF) in zy plane for the gold semishell structure from Fig.1b) (R_{out} = 100 nm, *d* = 20 nm, log scale): a) semishell with *h* = 20 nm (λ = 714 nm – EF maximum); b) *h* = 20 nm (λ = 589 nm – extinction maximum); c) *h* = 10 nm (λ = 718 nm – EF); d) *h* = 10 nm (λ = 589 nm – extinction); e) *h* = 0 nm (λ = 714 nm – EF); f) *h* = 0 nm (λ = 585 nm – extinction); g) *h* = -10 nm (λ = 722 nm – EF); h) *h* = -10 nm (λ = 585 nm – extinction); i) *h* = -20 nm (λ = 710 nm – EF); and j) *h* = -20 nm (λ = 581 nm – extinction); input x polarization.

As an additional design possibility, we have taken into account different way of opening of an open semishell structure. Instead of the parallel opening, we have also considered, inspired with preparation technique modification, conical opening (see Fig.1c)). Thus, instead of parameter *h*, the angle θ, defining the extent of opening of a semishell is used. In this sense, corresponding results are shown in Fig.3d) and e), again for the extinction, absorption, and scattering cross sections, for two choices of angle θ. Similarly, Figs.6 and 7 present the distributions of the EF in zx and zy planes, respectively (with the same notation and meaning as

previously). Again, corresponding hot spots appear in those parts of a structure close to the orientation of the input polarization. This structural opening ensures practically the same EF.

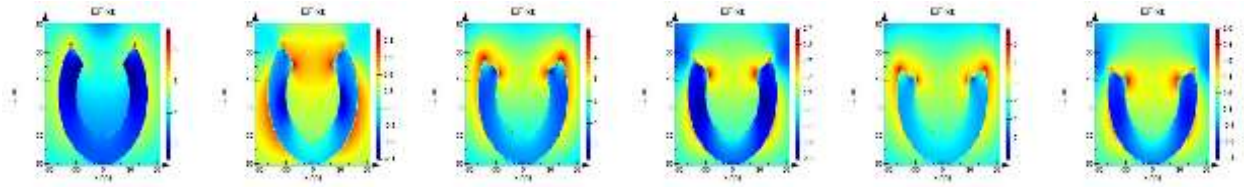

a) b) c) d) e) f)

Fig. 6: Field enhancement factors (EF) in zx plane for the gold semishell structure from Fig.1c) with conical opening (R_{out} = 100 nm, d = 20 nm, log scale): a) semishell with θ = 90 deg (λ = 795 nm – EF maximum); b) θ = 90 deg (λ = 577 nm – extinction maximum); c) θ = 120 deg (λ = 726 nm – EF); d) θ = 120 deg (λ = 589 nm – extinction); e) θ = 140 deg (λ = 726 nm – EF); f)) θ = 140 deg (λ = 593 nm – extinction); input x polarization.

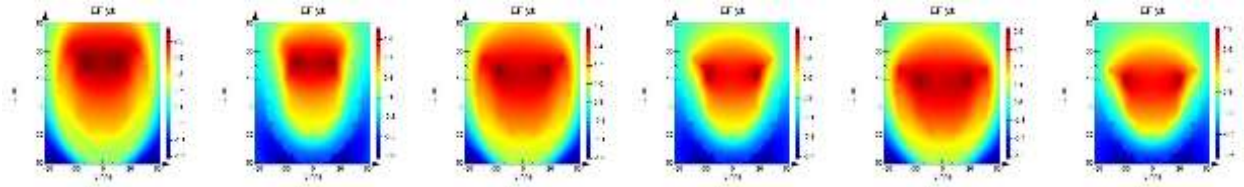

a) b) c) d) e) f)

Fig. 7: Field enhancement factors (EF) in zy plane for the same gold semishell structure from Fig.1c) with conical opening: a) semishell with θ = 90 deg (λ = 706 nm – EF maximum); b) θ = 90 deg (λ = 577 nm – extinction maximum); c) θ = 120 deg (λ = 722 nm – EF); d) θ = 120 deg (λ = 589 nm – extinction); e) θ = 140 deg (λ = 722 nm – EF); f)) θ = 140 deg (λ = 593 nm – extinction); input x polarization.

So far, the isolated structures were considered without any substrate, however, in a realistic situation, the substrate supporting semishells must be considered, typically made from silicon. It has turned out that the presence of such a silicon substrate, mounted with a single semishell structure, made field to concentrate not only on top edges of a semishell (as previously), but also close to the contact area with the substrate, thus slightly lowering the overall EF, as expected.

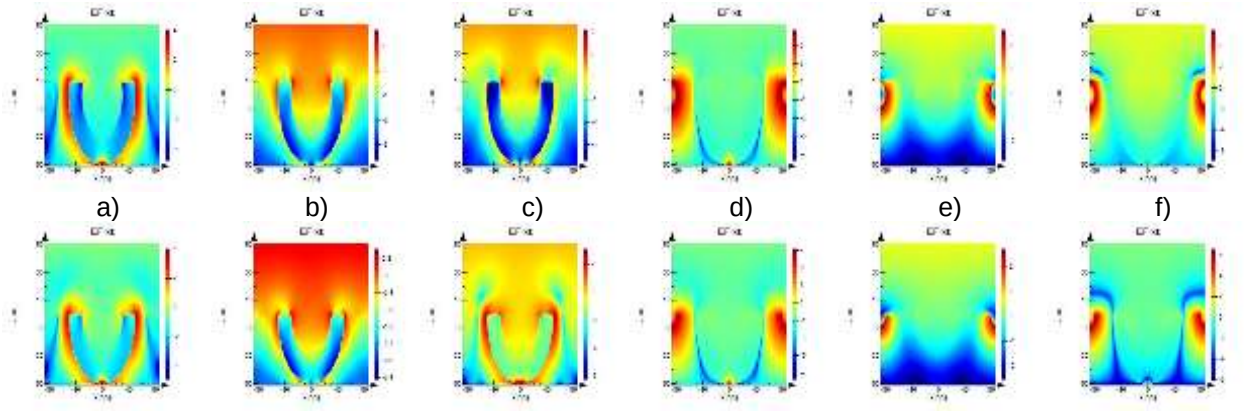

a) b) c) d) e) f)

g) h) i) j) k) l)

Fig. 8: Field enhancement factors (EF) in zx plane. Periodic array of closely packed semishells with parallel opening from Fig.1d) (individual shell diameter R_{out} = 100 nm, d = 20 nm, log scale), input field polarization along x (a), b), c), g), h), and i)) and y axis (d), e), f), j), k), and l)), with h = 10 nm (a), b), c), d), e), and f)) and h = 0 nm (g), h), i), j), k), and l)): a) λ = 906 nm – EF maximum; b) λ = 685 nm – reflectivity R maximum; c) λ = 807 nm – transmission T maximum; d) λ = 897 nm – EF maximum; e) λ = 676 nm – R maximum; g) λ = 793 nm – T maximum; g) λ = 911 nm – EF maximum; h) λ = 695 nm – R maximum; i) λ = 878 nm – T maximum; j) λ = 901 nm – EF maximum; k) λ = 685 nm – R maximum; l) λ = 864 nm – T maximum.

Next, out attention was given to arrays of semishell structures with hexagonal periodic arrangement (see Fig.1d)). In this case, the structure was considered already with Si substrate, in accordance with the realistic design. Based on the spectral behavior of reflection and transmission, we have again studied the corresponding field enhancement factors for the zx and zy planes, as shown in Fig.8 and 9, respectively.

Comparing the results of isolated and periodically arranged semishells, one can see that the strength of the EF is only slightly lowered, as compared to previous isolated case, reaching thus the highest values as ~10^4.

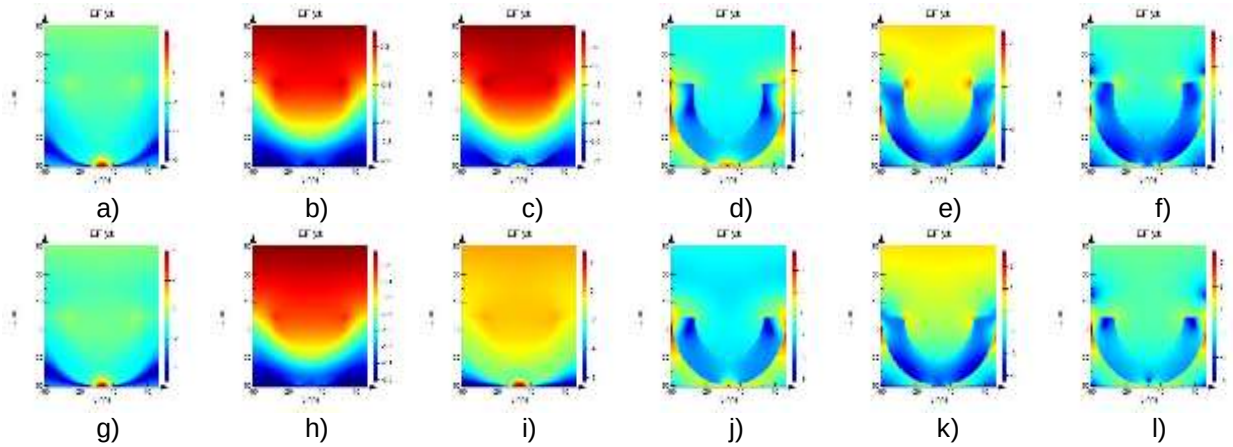

Fig. 9: Field enhancement factors (EF) in zy plane. Periodic array of closely packed semishells with parallel opening from Fig.1d) (individual shell diameter R_{out} = 100 nm, d = 20 nm, log scale), input field polarization along x (a), b), c), g), h), and i)) and y axis (d), e), f), j), k), and l)), with h = 10 nm (a), b), c), d), e), and f)) and h = 0 nm (g), h), i), j), k), and l)): a) λ = 906 nm – EF maximum; b) λ = 685 nm – reflectivity R maximum; c) λ = 807 nm – transmission T maximum; d) λ = 897 nm – EF maximum; e) λ = 676 nm – R maximum; g) λ = 793 nm – T maximum; g) λ = 911 nm – EF maximum; h) λ = 695 nm – R maximum; i) λ = 878 nm – T maximum; j) λ = 901 nm – EF maximum; k) λ = 685 nm – R maximum; l) λ = 864 nm – T maximum.

The second type of structures studied was (see Fig.1e) and f)), again inspired with the preparation technique, mastered in our department, a periodic array of gold triangles. As is seen in Fig.1e), the diameter of the original spheres directly determines the height (and thus size) of the gold triangle pedestal. The height of the whole 3D triangle is thus noted with the parameter v here. An example of the results is shown in Fig.10 where both reflection, transmission, and absorption (RTA) spectra (note the drop of transmission below 350 nm towards zero due to a silicon substrate) as well as the EF factor (for the normal incidence, input polarization along y axis) are presented. Again, we can see, similarly to the case of semishell structures, also for triangles, the EF as high as 10^5 is achievable in close vicinity of gold triangles.

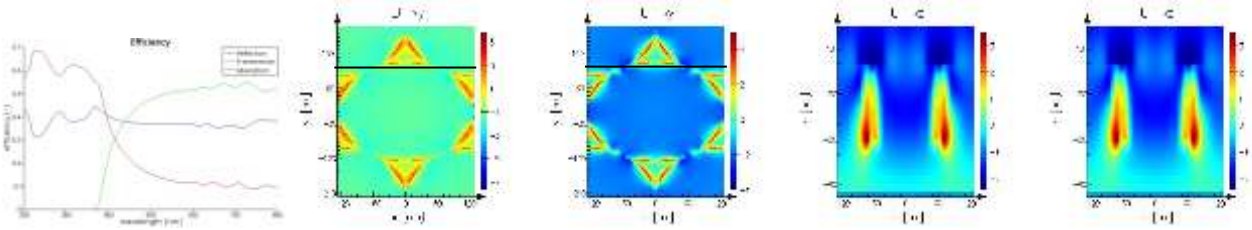

Fig. 10: Example of RTA spectrum and field enhancement (EF) factors for a gold nanotriangle structure from Fig.1 e) on a Si substrate: a) RTA spectrum; b) triangle height v = 50 nm, xy plane; c) triangle height v = 80 nm, xy plane; d) triangle height v = 50 nm, xz plane; e) triangle height v = 80 nm, xz plane. Diameter of the original sphere r = 253 nm. Log scales were used for the EF plots, black lines in a) and b) indicate the position of xz cuts, the corresponding wavelengths were tuned to EF maxima.

3. CONCLUSION

In summary, we have presented our new results on electromagnetic fully 3D simulations of two types of promising gold structures, performing as efficient and reproducible SERS substrates, namely: semishell and triangular structures. Previously, both these types of structures were experimentally prepared and successfully tested for their SERS performance in our laboratory, showing quite favorable behavior. Based on the FDTD electromagnetic calculations, we have thus been able to identify and describe both corresponding extinction cross section spectral dependences (for the case of isolated structures), as well as the spectral RTA behavior (in the case of hexagonally ordered periodic systems, not shown here, and gold triangle systems), in close correspondence to the field EF (of the order of 10^5 for both structures), veryfying also theoretically their potential for the amplification of SERS signals. Clearly, only the electromagnetic

enhancement was taken into account here. In this way, the morphology parameters for suitable SERS substrates could be optimized, ensuring best SERS performance. Also, it is possible to reveal, via such simulations, the correspondence to the overall SERS performance. By our rigorous numerical studies, we have thus partially contributed to better understanding of design strategies for advanced SERS substrates. Such numerical studies will be beneficial, in the next stage, in a direct interconnection with our corresponding laboratory preparation procedures and design strategies for advanced SERS substrates.

ACKNOWLEDGEMENTS

This work was partially supported by the Czech Science Foundation P205/13/20110S project.

REFERENCES

[1] MAIER, S. A. Plasmonics: Fundamentals and applications. New York: Springer, 2007

[2] RU, E. L. Principles of Surface Enhanced Raman Spectroscopy and related plasmonic effects. Amsterdam: Elsevier, 2009.

[3] CIALLA, D., MÄRZ, A., BÖHME, R., THEIL, F., WEBER, K., SCHMITT, M., POPP, J. Surface-enhanced Raman spectroscopy (SERS): progress and trends. *Analytical and Bioanalytical Chemistry*, vol. 403, 2012, p. 27-54.

[4] SCHULLER, J. A., BARNARD, E. S., CAI, W., JUN, Y. C., WHITE, J. S., BRONGERSMA, M. L. Plasmonics for extreme light concentration and manipulation. *Nature Materials*, vol. 9, 2010, p. 193-204.

[5] PELTON, M., AIZPURUA, J., BRYANT, G. Metal-nanoparticle plasmonics. *Laser & Photonics Reviews*, vol. 2, 2008, p. 136-159.

[6] HALAS, N. J., LAL, S., LINK, S., CHANG, W.-S., NATELSON, D., HAFNER, J.H., NORDLANDER, P. A. Plethora of plasmonics from the Laboratory for nanophotonics at Rice University. *Advanced Materials*, vol. 24, 2012, p. 4842-4877.

[7] CAO, Y., LI, D., JIANG, F., YANG, Y., HUANG, Z. Engineering metal nanostructure for SERS application. *Journal of Nanomaterials*, vol. 17, 2013, p. 123812:1-12.

[8] KNIGHT, M. V., HALAS, N. J. Nanoshells to nanoeggs to nanocups: optical properties of reduced symmetry core–shell nanoparticles beyond the quasistatic limit. *New Journal of Physics*, vol. 10, 2008, p. 105006:1-10.

[9] VAN DORPE, P., YE, J. Semishells: Versatile plasmonic nanoparticles. *ACS Nano*, vol. 5, 2011, p. 6774-6778.

[10] SU, Y., YE, S. HOU, Y., SHI, S., LI, S., Gao, F., DUA, J. Design and fabrication of diverse three-dimensional shell-like nano-structures. *Microelectronic Engineering*, vol. 115, 2014, p. 6–12

[11] YE, J., LAGAE, L., MAES, G., BORGHS, G., VAN DORPE, P. Symmetry breaking induced optical properties of gold open shell nanostructures. *Optics Express*, vol. 17, 2009, p. 23765-23771.

[12] KING, N.S., LI, Y., AYALA-OROZCO, C., BRANNAN, T., NORDLANDER, P., HALAS. N. J. Angle- and spectral-dependent light scattering from plasmonic nanocups. *ACS Nano*, vol. 5, 2011, p. 7254-7262.

[13] WANG, Y.X., LIU, S.S., GAO, W.T., LI, W., ZHANG, Y.J., YANG, J.H. Surface-enhanced Raman spectroscopy based on ordered nanocap arrays. *Superlattices and Microstructures*, vol. 52, 2012, p. 750–758

[14] DICKREUTER, M., GLEIXNER, J., KOLLOCH, A., BONEBERG, J., SCHEER, E., LEIDERER, P., Mapping of plasmonic resonances in nanotriangles. Beilstein Journal of Nanotechnology, vol. 4, 2013, p. 588-602.

[15] AWADA, C., POPESCU, T., DOUILLARD, L., CHARRA, F., PERRON, A., YOCKELL-LELIEVRE, H., BAUDRION, A.-L., ADAM, P.-M., BACHELOT, R. Selective Excitation of Plasmon Resonances of Single Au Triangles by Polarization dependent light Excitation, *Journal of Physical Chemistry C*, vol. 116, 2012, p. 14591-14598.

[16] ŠTOLCOVÁ, L., PROŠKA, J., NOVOTNÝ, F., PROCHÁZKA, M., RICHTER, I. Periodic arrays of metal nanobowls as SERS-active substrates. In Conference Proceedings *Nanocon 2011*. Brno: TANGER, 2011, p. 737-741.

[17] ŠTOLCOVÁ L., PROŠKA J., PROCHÁZKA M., Hexagonally ordered gold semishells as tunable SERS substrates. In Conference Proceedings *Nanocon 2012*. Brno: TANGER, 2012, p. 225-229.

[18] ŠTOLCOVÁ, L., PROŠKA, J., PROCHÁZKA, M. Rationally designed SERS substrates for the ultrasensitive detection of biologically important compounds. In Conference Proceedings *Nanocon 2012*. Brno: TANGER, 2013, p. 659-664.

[19] FUJIMURA, R., ZHANG, R., KITAMOTO, Y., SHIMOJO, M., KAJIKAWA, K. Modeling of semi-shell nanostructures formed by metal deposition on dielectric nanospheres and numerical evaluation of plasmonic properties. *Japanese Journal of Applied Physics*, vol. 53, 2014, 035201:1-4.

[20] Lumerical FDTD Solutions, Web source [https://www.lumerical.com/tcad-products/fdtd/]

[21] JOHNSON, P. B., CHRISTY, R.W. Optical constants of the noble metals. Physical Review B, vol. 6, 1972, p. 4370–4379.